Chemistry–A European Journal
Research Article
doi.org/10.1002/chem.202400585
Chemistry Europe
European Chemical Societies Publishing
www.chemeurj.org

VIP *Very Important Paper*

Formation of Peroxynitrite, $[O{-}N{-}O{-}O]^-$, via a Cascade of Reactions between Ozonide and Ammonia

Jonas R. Schmid,[a] Oliver R. H. Rennefeld,[a] Anja Wiesner,[a] Martin Jansen,*[b] and Sebastian Riedel*[a]

We report on an unexpected reaction between ammonia and potassium ozonide dissolved in liq. NH_3 resulting in the formation of peroxynitrite, $[ONOO]^-$, which exclusively happens in the presence of a specific partially fluorinated aniline-based ammonium cation. High-resolution structural data of the peroxynitrite anion in *cis*-conformation have been obtained. We further studied this molecule anion by single crystal Raman spectroscopy. The *cis* and *trans* isomers of peroxynitrite were analysed computationally with respect to their relative energies, the *cis-trans* transition barrier and their decomposition pathways to the nitrate anion. By experimentally examining cations decorated with fluorine ligands to different degrees, we demonstrate that fluorine specific interactions play a crucial role in the unexpected formation of peroxynitrite and as a conspicuously structure directing factor for the underlying crystalline solid phases, exhibiting distinct micro-separations of fluorine and hydrogen enriched regions.

Introduction

The ozonide ion features a bunch of intriguing chemical characteristics, which enable to function as a Lewis or Brønstedt base, to undergo radical recombination reactions, to act as a donor ligand in coordination chemistry, and to release highly reactive mono-oxygen. As a less favourable consequence of such high and versatile reactivities, preparing and handling bulk samples of ionic ozonides pose particular challenges.[1] The initial step in accessing this class of compounds is a gas-solid reaction of ozone with heavy alkali metal superoxides, followed by extraction of the respective ozonide from the raw product with liquid ammonia.[2] From the alkali metal ozonides obtained along this route, ionic ozonides of virtually any other monovalent single atomic or complex cation is attainable via metathesis[3] or ion exchange reactions[4] in liquid ammonia.

While the puzzling observation of substantial variations of O–O bond lengths and O–O–O bonding angles has been revealed to be a result of electrostatic crystal field effects[5] or C–H···O hydrogen bonding,[6] both polarising the weakly bonded electrons in the $2b_1$ anti-bonding HOMO, the promising synthetic potential of the ozonide anion has remained unexplored, so far. Radical recombination, i.e., dimerization to form $(O_6)^{2-}$ in analogy to the behaviour of the $(S_3)^-$ radical anion, is among the first options that come to mind. However, neither lowering temperature (which works with the sulphur homologue) nor increasing concentration has been effective in the sense of such an expectation, so far.

The motivation behind the study presented here has been to enforce spatial proximity and possibly dimerization of the ozonide radical ions in a solid phase by employing tools of crystal engineering. It is well known that crystal structures of molecular species decorated with fluorine and hydrogen in specific patterns display a kind of internal microscopic phase separation. Driven by the effect of „similars are attracting similars", contact regions form that are either dominated by fluorine or by hydrogen. Our concept to prompt dimerization of the $(O_3)^-$ species in the solid state is based on this phenomenon. Crystallizing ozonides of complex ammonium cations, where one hemisphere is furnished predominantly with fluorine ligands, the other with hydrogen atoms, would affect the fluorine peripheries to flock together and the ozonide anion to assemble in a confined space close to the hydrogen enriched regions.[7] The latter would further represent areas of highest positive potential. The cation $[NMe_3(C_6H_3(CF_3)_2)]^+$, **1**, chosen for a first trial, is shown in Scheme 1.

Commonly, solutions of such ammonium ozonides in liquid ammonia are stable.[1] However, quite as a surprise, the red colour of freshly prepared solutions of $[NMe_3(C_6H_3(CF_3)_2)]O_3$, **2**, vanishes irrespective of the counter-anion ($[BF_4]^-$ or $[SO_3CF_3]^-$) present and whether the ion exchange or metathesis procedure was applied, indicating that some unexpected reaction had happened. Indeed, at processing the product solution by slowly evaporating the solvent, a single phase material crystallized, which has been identified as the respective peroxynitrite, $[NMe_3(C_6H_3(CF_3)_2)][ONOO]\cdot 1/3\ NH_3$, **3**. We claim that the final

[a] J. R. Schmid, O. R. H. Rennefeld, Dr. A. Wiesner, Prof. Dr. S. Riedel
Anorganische Chemie, Institut für Chemie Biochemie
Freie Universität Berlin
Fabeckstraße 34/36
14195 Berlin, Germany
E-mail: s.riedel@fu-berlin.de

[b] Prof. Dr. Dr. h.c. M. Jansen
Max-Planck-Institut für Festkörperforschung
Heisenbergstraße 1
70569 Stuttgart, Germany
E-mail: m.jansen@fkf.mpg.de

Supporting information for this article is available on the WWW under https://doi.org/10.1002/chem.202400585

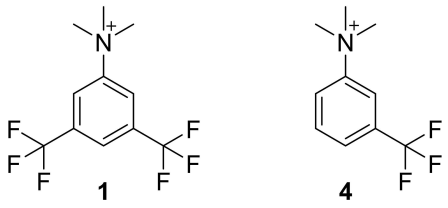

Scheme 1. Partially fluorinated cations for the stabilization of reactive oxygen-based anions.

step of a cascade of reactions, all between species immanent to the system, corresponds to a biomimetic radical combination of NO and $(O_2)^-$.[8] As another hard to rationalize incidence, this conspicuous reaction sequence seems to exclusively occur in presence of cation **1**. Even the slight change of removing one of the $-CF_3$ substituents from the cation's periphery (**4**, Scheme 1) suppresses the exotic outcome ($[ONOO]^-$ formation), and the respective ozonide shows the ordinary behaviour.

Results and Discussion

Phenomenological Observations

Solutions of the targeted ionic ozonide $[NMe_3(C_6H_3(CF_3)_2)]O_3$ in liquid ammonia, as prepared along the standard ion exchange route (dissolution of KO_3 in liquid ammonia in a special glass apparatus in the presence of the desired cation as dissolved salt or loaded onto an ion exchange resin at low temperatures)[4] rapidly change the characteristic deep red colour of $(O_3)^-$ to pale yellow. This clearly testifies disappearance of the red ozonide anion. Different from the common decomposition reaction of the ozonide species, no evolution of gaseous oxygen was observed. By slowly cooling the solvent to −77 °C, a pale yellow solid crystallised. Characterization by single crystal x-ray diffraction revealed the formation of peroxynitrite **3**. This finding is without precedent and hard to rationalise. To demonstrate that the formation of the peroxynitrite depends on the chosen cation, we changed the complex ammonium cation by just replacing one $-CF_3$ group by –H. Astoundingly, even such an apparently modest variation of the periphery of the cation restored the common reaction path and the respective ozonide, $[NMe_3(C_6H_4(CF_3))]O_3$, **5**, was obtained.

Crystal Structures of $[NMe_3(C_6H_3(CF_3)_2)][ONOO]\cdot 1/3\ NH_3$ and $[NMe_3(C_6H_4(CF_3))]O_3$

As a conspicuous outcome of our study, we note the strongly directing impact of the distinct grading of the dispersion interactions between the ammonium cations, in solution as well as in the solid state. This is clearly evident from the formation and arrangement of rods, substantially driven by so called "fluorophilic interactions"[9] where fluorine bearing substituents flock together forming the total or part of the rod shells in **3** or in **5**, respectively. These 1D units arrange to hexagonal dense rod packings, and the resulting crystal structures of both, **3** and **5**, correspond to the hexagonal phases known from lyotropic liquid crystalline phases as formed by tenside molecules in water[10] or liquid ammonia,[11] see Figures 1 and 2.

For **3**, we identify strands of cation/anion pairs as secondary building units (see Supporting Information, SI, Figure S6), which are replicated by the 6_3 symmetry axis to form the rods mentioned.

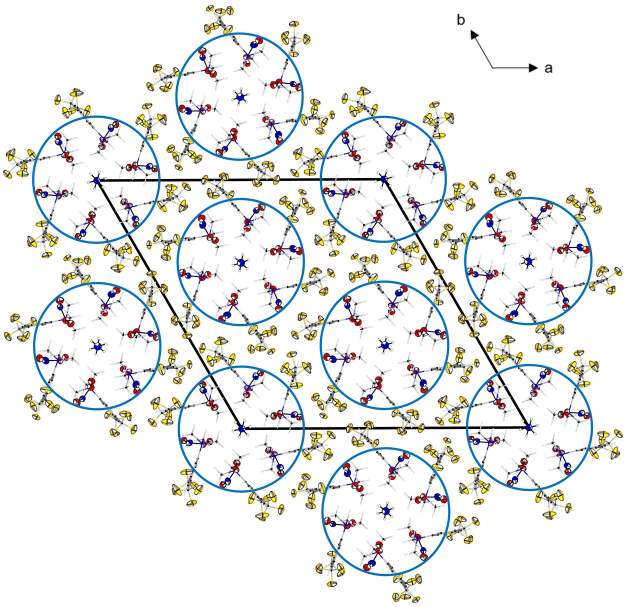

Figure 1. Projection of the crystal structure of $[NMe_3(C_6H_3(CF_3)_2)][ONOO] \bullet 1/3\ NH_3$ along [001]. Margins of the unit cell are shown in black, blue circles highlight the hexagonal dense rod packing. Fluorine, peroxynitrite and ammonia are presented as thermal ellipsoids set at 70% probability level, all other atoms are drawn in wire and stick representation. Hydrogen in white, nitrogen in blue, carbon in grey, fluorine in yellow and oxygen in red colour.

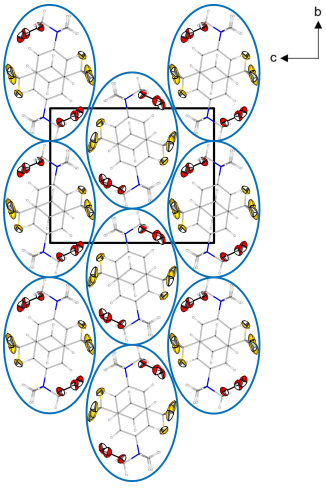

Figure 2. Projection of the crystal structure of $[NMe_3(C_6H_4(CF_3))]O_3$ along [100]. Except fluorine and oxygen, all atoms are represented as wire and stick representation. Thermal ellipsoids for all other atoms are set at 70% probability level. Hydrogen in white, nitrogen in blue, carbon in grey, fluorine in yellow and oxygen in red colour. Rotational CF_3 disorder and $(O_3)^-$ disorder is omitted for clarity.

As a consequence, protonic regions and the positive potentials of the ammonium cations accumulate around the centres of the cylindrical building units, which are occupied by the solvent ammonia. Within these regions of highest positive potential, concurrently including all potential donors for hydrogen bonding, the peroxynitrite anions are located. The columns in **5** consist of stackings of the cations alone, see Figure 2, while the ozonide ion is accommodated in the interstitial space (Figures S8 and S9). Further details of the crystal structure of 5 are discussed in SI.

Table 1. Crystal and structure refinement data for

Sum formula	$C_{33}H_{39}F_{18}N_7O_9$	$C_{10}H_{13}F_3NO_3$
Space group, Z	$P6_3$ (No.173), 6	$P2_12_12_1$ (No.19), 4
a/Å	27.5463(5)	7.325(2)
b/Å	27.5463(5)	11.207(2)
c/Å	9.5302(3)	13.649(3)
Volume/Å^3	6262.7(3)	1120.5(3)
Temperature/K	104	100
ρ_{calc} g/cm^3	1.622	1.495
Diffractometer	Bruker D8-Venture	Bruker D8-Venture
Radiation	CuKα (λ = 1.54178)	CuKα (λ = 1.54178)
2Θ range for data collection/°	3.704 to 140.924	10.212 to 136.352
Index ranges	$-32 \le h \le 28$, $-29 \le k \le 31$, $-10 \le l \le 10$	$-8 \le h \le 8$, $-13 \le k \le 12$, $-15 \le l \le 14$
Reflections collected	55643	10858
Independent reflections	7318 [R_{int} = 0.0594, R_{sigma} = 0.0404]	1982 [R_{int} = 0.0492, R_{sigma} = 0.0386]
Data/restraints/parameters	7318/1/625	1982/63/214
Goodness-of-fit on F^2	1.077	1.049
Final R indexes [all data]	R_1 = 0.0597, wR_2 = 0.1041	R_1 = 0.0617, wR_2 = 0.1630
Largest diff. peak/hole/e Å^{-3}	0.45/−0.28	0.24/−0.29
Flack parameter	0.5	

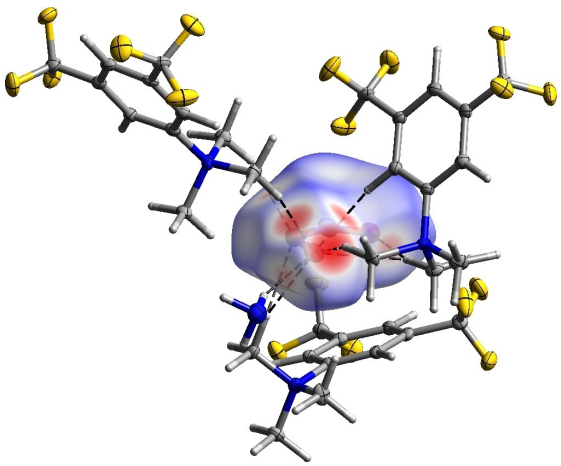

Figure 3. Hirshfeld surface of one of the three crystallographic independent peroxynitrite anions in **3**. Hydrogen bonds are visualized as dotted lines. Thermal ellipsoids are set at 50% probability.

The crystallographic data of both the crystal structure analyses are given in Table 1, respective atomic parameters as well as relevant distances and angles are given as Tables S1–S12 in SI.

The embedding of the complex anion $[ONOO]^-$ in the extended solid is basically controlled by electrostatic interactions with the ammonium centres of three adjacent complex cations, and by hydrogen bonding, in particular to the solvent ammonia molecule, see Figure 3. The hydrogen bonds towards oxygen atoms in **3** with respect to the labeling e in Figure 5 for the three crystallographically independent peroxynitrites range from O1 = 251.9(4) to 257.6(4) pm, O2 = 241.7(5) to 255.5(3) pm and O3 = 217.4(3) to 254(5) pm.

In all cases, the strongest and majority of hydrogen bonds arrive at the terminal oxygen atom O3, which agrees well with the electrostatic potential plotted on the isosurface of the electron density for peroxynitrite (Figure 4). No hydrogen bonds towards the nitrogen atom are present.

The crystal structure determination on **3** has revealed the structure of the peroxynitrite anion in high precision, see Figure 5; while the quality of respective data reported previously suffer from problems caused by orientational disorder.[12] The bond lengths observed here can be understood in terms of qualitative concepts. The distance O1–N1 corresponds to a double bond, while the N1–O2 and O2–O3 distances are

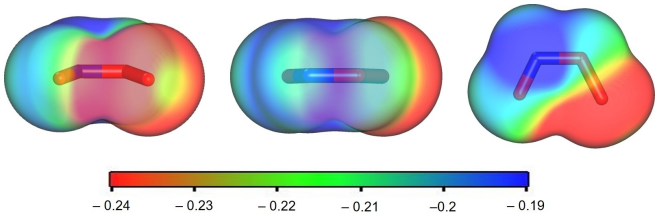

Figure 4. Electrostatic potentials of *cis* $[ONOO]^-$ in the range of −0.24 a.u. (red) to −0.19 a.u. (blue) are mapped onto their electron densities (isosurface value 0.0035 a.u.); calculated at the B3LYP-D3(*BJ*)/aug-cc-pVTZ level of theory (Gaussian 16) in the gas phase.

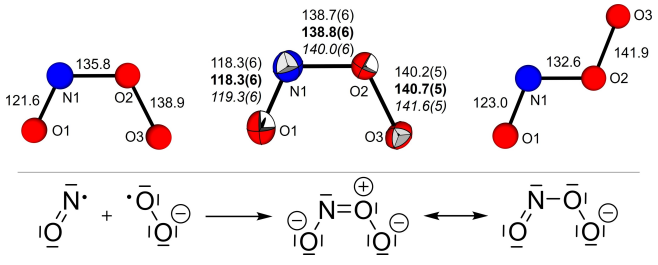

Figure 5. Calculated and experimental bond lengths for the peroxonitrite anion. Middle, experimental data for the three crystallographic independent species (see Table S5). Left and right, calculated values for the cis and trans conformers, respectively, calculated at CCSD(T)/aug-cc-pVQZ level of theory (Orca 5.0.3). Thermal ellipsoids set at 50% probability. Selected angles in **3** are O1–N1–O2 = 114.0(4), 114.1(5) and 114.4(4) °, N1–O2–O3 = 115.7(4), 116.3(3) and 116.3(4) ° for the three crystallographic independent anions. The dihedral angles are ranging from O1–N1–O2–O3 = −1.3(6), −0.7(8) and 1.3(6) °. Lower trace: Formation of $[ONOO]^-$ by radical recombination and two resonance structures.

indicative of single bonds. This suggests that the negative charge is located at O3. For a detailed quantitative analysis of the bonding properties of $[ONOO]^-$ see next section.

Reaction Path Towards Peroxynitrite

As the colour of freshly prepared solutions of $[NMe_3(C_6H_3(CF_3)_2)]O_3$ in liquid ammonia rapidly changes from deep red to pale yellow, it is evident that the peroxynitrite anion forms in solution; any solid-state effect or selection by the much longer lasting process of crystal growth can thus be excluded. The seemingly unexpected formation of the peroxynitrite anion has to be understood in terms of species that are immanent to the system studied. Significant amounts of foreign species can be reliably excluded, since absence of impurities has to be ensured meticulously during any operation involving the highly reactive ozonide ion. Respective measures were taken in all experiments reported here. The solution under consideration consists of $[NMe_3(C_6H_3(CF_3)_2)]^+$ and $(O_3)^-$, dissociated in $NH_{3,\,liq.}$.

The literature known synthesis of peroxynitrite $[ONOO]^-$ is the radical combination NO and $(O_2)^-$ (Scheme 2).[8a,12,13] In our system, homogeneous equilibria according to equations (1) to (6) may establish. Therefore, we propose the following mechanism for our system: As a result of the exothermic decomposition of the ozonide anion (−23 kJ/mol from recorded data),[14] mono-oxygen and a superoxide anion are formed (Eq. 1). The mono-oxygen reacts with the solvent ammonia to form hydroxylamine (Eq. 2), followed by an additional oxidation (Eq. 3). In the next step HNO is formed under water (water traces would immediately react with residual ozonide or superoxide) abstraction (Eq. 4). HNO will easily cleave into $^{\bullet}H + {}^{\bullet}NO$ (eq. 5), in accordance with the low experimental binding energy 196.2 ± 0.4 kJ/mol (calculated: 203.9 kJ/mol).[15] The intermediate mono hydrogen radicals may combine to form H_2 or react with other radical species ($(O_2)^-$ and $(O_3)^-$) present. Alternatively, the latter may abstract hydrogen directly from HNO. The last step in the reaction cascade is the exothermic radical combination (−95 kJ/mol at CCSD(T)/aug-cc-pVQZ) to form $[ONOO]^-$ (Eq. 6).

This reaction path has been corroborated by total energy calculations, which clearly indicate that the mechanism assumed appears to proceed under thermodynamic control at each step (Scheme 3). However, no reaction barriers were investigated as these should be relatively small for radical reactions. The reaction steps were calculated at B3LYP-D3(*BJ*)/aug-cc-pVTZ level of theory with a conductor-like polarizable continuum model with COSMO dielectric constant for ammonia (CPCMC(NH_3)).

In particular, enhancing the acidity of ammonia by coordination to a Lewis acidic cation with an ion strength higher than the one of the heavy alkali cations (K, Rb, Cs) has been shown to induce the decay of $(O_3)^-$, even at low temperature. For this reason, crystalline NaO_3 cannot be harvested unless ammonia is replaced by methylamine.[16] Therefore, we investigated the ammonia cation interaction of **1** and **4** in comparison with the related non-fluorinated cations by quantum-chemical calculations (for details see SI, Chapter 4.1). As expected, the higher degree of fluorination of the aniline-based cations results in a stronger interaction. The strongest interactions were observed for $[NMe_3(C_6H_3(CF_3)_2)]^+$ in the 2 and 6 position of the aromatic ring, which, however, are significantly weaker than Na^+ ammonia interactions. By plotting the electrostatic potential on the isosurface of the electron density for all investigated cations an anisotropic distribution of the potential is observed. Furthermore, the localisation of the positive partial charge at the 2 and 6 position of the cations **1** and **4** increases compared with the related non-fluorinated cations, making these positions more accessible for an interaction with ammonia or ozonide. This phenomenon is further amplified when an SMD solvent model for ammonia is used,[17] which enhances the localized charge in these cations (B3LYP-D3(*BJ*)/aug-cc-pVTZ level of theory, Figure S28, S29). Based on these results, we assume that the cation interactions are decisive for the formation of peroxynitrite. To exclude a possible influence of the nature of the anion in the formation of $[NMe_3(C_6H_3(CF_3)_2)][ONOO]$ we varied the original approach of starting from $[NMe_3(C_6H_3(CF_3)_2)][BF_4]$ and KO_3. Employing the triflate salt $[NMe_3(C_6H_3(CF_3)_2)][SO_3CF_3]$ instead of the tetrafluoroborate, at otherwise identical reaction conditions, resulted in an analogous outcome, i.e. the formation of peroxonitrite. We conclude

Bohle 1994:

$$[NMe_4]O_2 + {}^{\bullet}NO \xrightarrow[NH_3]{} [NMe_4][ONOO]$$

This work:

$$2\,(O_3)^{-\bullet} \longrightarrow 2\,(O_2)^{-\bullet} + 2\,O \quad (1)$$

$$NH_3 + O \longrightarrow H_3NO \longrightarrow H_2NOH \quad (2)$$

$$H_2NOH + O \longrightarrow H_2N(O)OH \quad (3)$$

$$H_2N(O)OH \longrightarrow HNO + H_2O \quad (4)$$

$$HNO \longrightarrow H^{\bullet} + {}^{\bullet}NO \quad (5)$$

$${}^{\bullet}NO + (O_2)^{-\bullet} \longrightarrow [ONOO]^- \quad (6)$$

$$2\,(O_3)^{-\bullet} + NH_3 \longrightarrow [ONOO]^- + H_2O + H^{\bullet} + (O_2)^{-\bullet}$$

Scheme 2. Possible reaction pathways towards the peroxynitrite compared to the literature known synthesis.[8a]

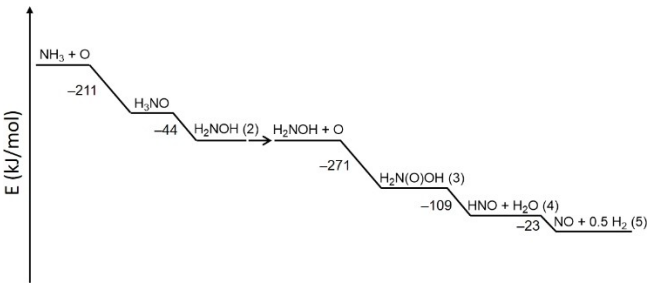

Scheme 3. Reaction scheme for the in-situ formation of NO from ammonia and mono-oxygen at B3LYP-D3(*BJ*)/aug-cc-pVTZ CPCMC(NH_3) level of theory (ORCA 5.0.3).

that the counter-anion used has probably no relevant influence on the reaction. To verify that ammonia acts as the nitrogen source, we repeated the reaction in methylamine, since it is less proton acidic than ammonia. After three months no discoloration of the ozonide was observed, showing that the decomposition only takes place in the presence of ammonia. Further, the stability of the cation towards ammonia was investigated to ensure that the fluorinated cation would not methylate the ammonia to form $[NMeH_3]^+$. The possibly formed methylammonium cation could initiate the decomposition of the ozonide, as observed for $[NH_4]O_3$ into ammonium nitrate.[18] For this purpose, $[NMe_3(C_6H_3(CF_3)_2)][SO_3CF_3]$ was exposed for 1 day to the autogenous pressure of anhydrous ammonia at room temperature. Subsequent slow cooling allowed the salt to be recovered as single crystals (Figure S15) and low temperature NMR experiments in liquid ammonia showed that no decomposition of the cation had occurred (Figure S25 and S26). Additionally, $[NMe_3(C_6H_3(CH_3)_2)]O_3$ was prepared to rule out the possibility that the structural directing properties of the cation are necessary for the formation of the $[ONOO]^-$ ion and was analysed by single crystal X-ray diffraction (Figure S12).

In spite of these empirical insights, we are unable to provide a conclusive explanation why peroxynitrite emerges from solutions of ozonide in liquid ammonia only in presence of the multiply fluorine substituted cation **1**. Obviously, understanding the activation of either ammonia or the ozonide anion in the first reaction step constitutes the key issue. Most probably, the electron rich ozonide anion gets attracted and activated by association to the electron poor phenyl ring of **1**.

The Bonding Properties of the Peroxynitrite Anion

As proven by the crystal structure determination of **3** the anion shows a planar conformation. This is also in agreement with our quantum-chemical calculations, see Figure 5, which indicates a significant π-type delocalization that extends over the entire anion.

By performing NBO (Natural Bond Orbital) in combination with NRT (Natural Resonance Theory) analysis on the resonance structures of both isomers, we show that there is a partial double bond character between the nitrogen N1 and oxygen atom O2 (*cis* = 27%, *trans* = 31%) and a partial double (*cis* = 21%, *trans* = 30%) and triple bond (*cis* = 13%, *trans* = 14%) between N1 and O1 (Figure 6). The resonance structures for both isomers show additionally an interaction of the terminal oxygen atoms O1 and O3, which can take place via the backbone of the molecule or via the free electron pairs which point above and below the N–O2 axis.

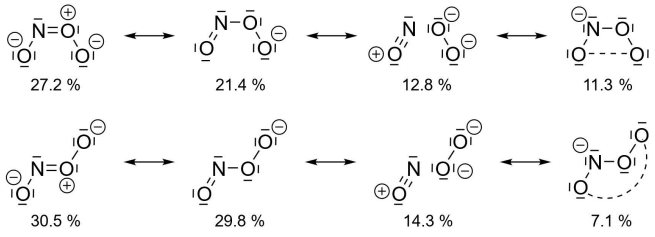

Figure 6. Natural resonance structures of the *cis* and *trans* isomer of $[ONOO]^-$ at B3LYP-D3(*BJ*)/aug-cc-pVTZ level of theory (Gaussian 16).

QTAIM (Quantum Theory of Atoms in Molecules) was applied to investigate both $[ONOO]^-$ conformers. The Laplacians of the electron density ($\nabla^2\rho$) at the bond critical points in the $[ONOO]^-$ isomers indicate a covalent character for all bonds in the cis isomer, from which the trans isomer differs by a more ionic bonding character for the O2–O3 bond (see supporting information, Chapter 4.5). Based on quantum-chemical calculations at CCSD(T)/aug-cc-pVQZ level of theory and in agreement with the literature[19] the *cis* isomer is energetically preferred by −14.4 kJ/mol compared to the *trans* isomer, (for technical details see SI, Table S31 and chapter 4.6). The *cis-trans* interconversion was evaluated via a relaxed dihedral surface scan with inclusion of solvent effects and without, see Figure 7. The energetic barrier for the interconversion amounts to 112 kJ/mol and 103 kJ/mol (CPCMC (NH_3)), respectively (Figure 7). These relative high barriers are due to the above mentioned partial double bond character of the N1–O2 bond which hinders the interconversion.

Additionally, the decomposition pathways of both isomers towards the more stable nitrate were investigated at B3LYP-D4/aug-cc-pVQZ level. Due to the energetically more favourable rotation of the N1–O2 bond in the *cis* isomer, in contrast to the strong O2–O3 bond extension in the *trans* isomer, the energy of the transition state is lower in the *cis* isomer by ca. 30 kJ/mol (see SI, Chapter 4.7).

Raman and IR Spectroscopy

The single crystal Raman spectrum of **3** (Figure 8) shows a band at 617 cm^{-1} which can be assigned to the peroxynitrite N1–O2 stretching mode which is in good agreement with quantum-

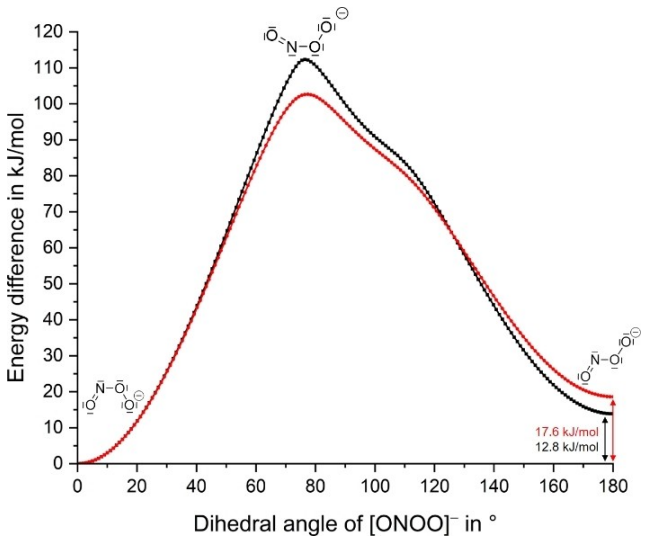

Figure 7. Relaxed dihedral surface scan (0–180° in 1° steps) with solvent module CPCMC(NH_3) (red) and level without (black) at B3LYP-D3(*BJ*)/aug-cc-pVTZ level of theory (Orca 5.0.3).

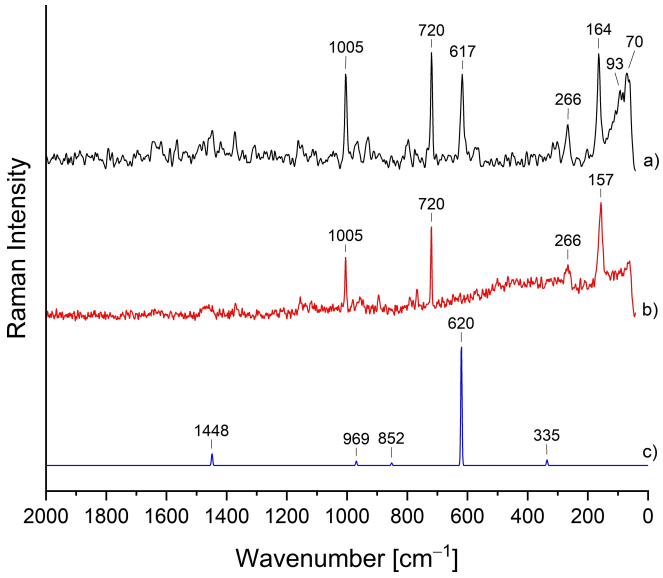

Figure 8. Comparison of the measured and calculated Raman spectra of the *cis* $[ONOO]^-$ ion ((a) Raman spectrum of $[NMe_3(C_6H_3(CF_3)_2)][ONOO] \bullet 1/3\ NH_3$ at −196 °C, (b) Raman spectra of $[NMe_3(C_6H_3(CF_3)_2)][BF_4]$ at r.t. and calculated Raman spectrum of *cis* $[ONOO]^-$ ion at B2PLYP/aug-cc-pVQZ level of theory using Orca 5.0.3).

chemical calculations (B2PLYP/aug-cc-pVQZ) and literature values for an aqueous system (642 cm^{-1}).[20] Additional anion specific bands were not observed due to the low intensity. All other bands can be assigned to the cation based on a reference spectrum of $[NMe_3(C_6H_3(CF_3)_2)][BF_4]$.

The IR spectrum (Figure 9) shows a weak absorption at 1530 cm^{-1} which can be assigned to the N1–O1 stretching mode which agrees well with literature values (1564 cm^{-1}). The

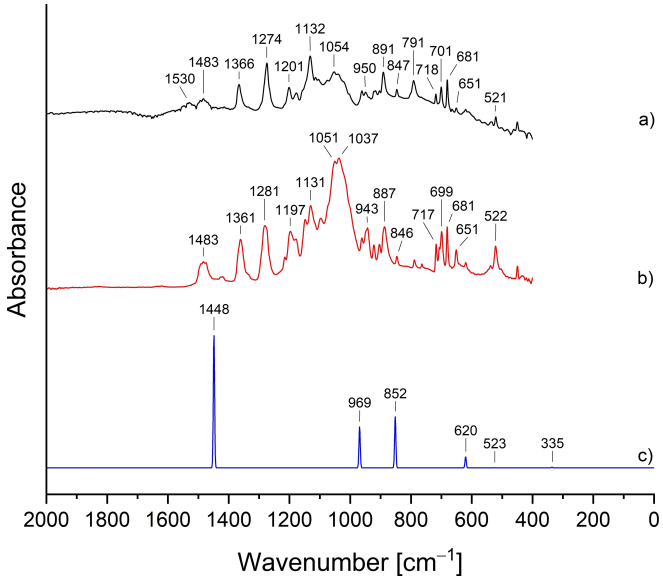

Figure 9. Comparison of the measured and calculated IR spectra of the *cis* $[ONOO]^-$ ion ((a) IR spectrum of $[NMe_3(C_6H_3(CF_3)_2)][ONOO] \bullet 1/3\ NH_3$ at −70 °C, (b) spectrum of $[NMe_3(C_6H_3(CF_3)_2)][BF_4]$ at r.t. and (c) calculated IR spectrum of *cis* $[ONOO]^-$ ion at B2PLYP/aug-cc-pVQZ level of theory using Orca 5.0.3).

quantum- chemically calculated spectrum (B2PLYP/aug-cc-pVQZ) shows a shift to lower wavenumbers for the NO stretching mode as well as a higher intensity compared to the measured spectrum. These deviations could be a result of multiple interactions in the solid-state compared to gas-phase calculations.[20–21] A comparable low IR intensity of the NO band in the solid state in contrast to the gas phase has been found for NO^+ salts.[22] All other bands can be assigned to the cation based on a reference spectrum of $[NMe_3(C_6H_3(CF_3)_2)][BF_4]$.

Quantum-chemical frequency calculations in the gas phase show a strong shift of the bands depending on the functional and the basis set, according to the chosen methods for the description of the peroxynitrite. It was shown that, more consistent results were obtained by QM/MM simulations of peroxynitrite in water. These results are in reasonable agreement with our ammonia system, even though calculated for an aqueous system.[23] Different functionals were tested for the description of the peroxynitrite and can be found in the supporting information (Table S24–S27).

Conclusions

In summary, we have shown that an unusual reaction occurs between ammonia and ozonide in the presence of a partially fluorinated $[NMe_3(C_6H_3(CF_3)_2)]$ cation. For the first time it was possible to obtain high resolution structural data of the peroxynitrite ion and to study it by single crystal Raman spectroscopy. Both the *cis* and *trans* isomer of the peroxynitrite were in depth investigated by quantum-chemical calculations as well as their decomposition pathway towards the nitrate. Furthermore, fluorine specific interactions induse a lyotropic liquid crystalline phase in the more uncommon space group $P6_3$.

Experimental Section

CAUTION! Strong oxidizers!

Ozonides are strong oxidizers and can lead with organic material to violent reactions. Strong friction can cause violent reactions. All reactions should be conducted under rigorously anhydrous conditions.

Materials, Chemicals and Procedures

All water and air sensitive substances were handled under Argon (Ar 5.0) atmosphere using standard Schlenk techniques and a vacuum up to 10^{-3} mbar. If not mentioned otherwise, all syntheses were performed under stated conditions. All glassware was flame dried and joints were sealed with Triboflon grease. Ammonia (3.8 Linde) was dried by refluxed over NaK overnight, distilled and stored in a dried stainless-steel gas cylinder. Single crystals were picked at −80 °C under nitrogen atmosphere and mounted on a 0.15 mm Mitegen micromount using perfluoroether oil diluted with perfluorohexane. Crystal data were collected on a Bruker D8 Venture diffractometer with a Photon II area detector or Photon III area detector with CuKα or MoKα radiation at 100(1) K or 104(1) K. Multiscan absorption correction was used as implemented in APEX

IV (SADABS-2016/2).[24] The structures were solved with the ShelXT[25] structure solution program using intrinsic phasing and refined with the ShelXL[26] refinement package using least squares minimizations by using OLEX2.[27] Hydrogen atoms were refined using HFIX 137 (CH_3) HFIX 43 ($C_{sp2}H$) as implemented. For visualization the Diamond V4.65 program package was used.[28] Raman spectra were recorded at r.t. and −196 °C on a Bruker MultiRAM II and Ramanscope equipped with a low-temperature Ge detector (1064 nm, up to 450 mW, resolution 4 cm^{-1}). IR spectra were recorded on a Nicolet iS50 Advance FTIR by Thermo Fisher Scientific equipped with an ATR unit, with a Ge on KBr beamsplitter and a DLaTGS-KBr detector for MIR and a solid-substrate beamsplitter with a DLaTGS-PE detector for FIR. For low-temperature measurements a metal cylinder cooled by a cold N_2 stream was used.

Raman and IR spectra were processed using OPUS 7.5[29] and Origin Pro 2022[30] was used for their graphical representation.

NMR spectra were recorded on a JEOL 600 MHz ECZ and JEOL 400 MHz ECS spectrometer. All reported chemical shifts are referenced to the Ξ values given in IUPAC recommendations of 2008 using the ^2H signal of the deuterated solvent as internal reference.[31] MestReNova 14.3 was used for processing the spectra and for their graphical representation.[32]

Quantum chemical calculations were conducted using the HPC system provided by the ZEDAT (Freie Universität Berlin, Curta).[33] The programs Orca 5.0.3, Orca 5.0.4[34] and Gaussian 16[35] were used in combination with the B3LYP-D3(*BJ*),[36] B3LYP-D4,[36a,b,37] B2PLYP[38] and PBE0-D3(*BJ*) functionals,[36c,d,39] CCSD(T)[40] method and aug-cc-pVTZ or aug-cc-pVQZ as basis set.[41] Natural resonance structures were calculated using NBO 7.0[42] in Gaussian 16 and transition states were calculated with the NEB-TS module implemented in ORCA 5.0.4.[43] Hirshfeld surfaces were visualized with Crystal Explorer 21[44] and electronic potentials mapped onto electron densities were visualized with VMD 1.9.3.[45]

KO_3

The compound was synthesized as described elsewhere.[2a]

$[NMe_3(C_6H_3(CF_3)_2)][BF_4]$

The compound was synthesized as described elsewhere.[46]

$[NMe_3(C_6H_3(CH_3)_2)]I$

The compound was synthesized as described elsewhere.[46]

$[NMe_3(C_6H_3(CF_3)_2)][SO_3CF_3]\cdot 1/2\ NH_3$:

The compound was synthesized as described elsewhere[47] and crystalized by cooling an ammonia (3 mL) solution of $[NMe_3(C_6H_3(CF_3)_2)][SO_3CF_3]$ (60 mg) in an ampule from r.t. to −77 °C.

$[NMe_3(C_6H_3(CF_3)_2)][ONOO]\cdot 1/3\ NH_3$

An H-shaped glass apparatus with a glass filter sieve of porosity 3 in the connection between the legs was charged with N,N,N-trimethyl-3,5-bis(trifluoromethyl)benzenaminium tetrafluoroborate (100 mg, 0.37 mmol, 1 equiv.) and potassium ozonide (ca. 100 mg, 1.15 mmol, 3.1 equiv.). Afterwards, ammonia (ca. 15 mL) was condensed onto the solids at −196 °C and the mixture was allowed to warm to −60 °C to fully dissolve the ozonide, resulting in a yellow-orange solution. The solution was stored at −76 °C for 3 days and extracted 1 time as described before.[4] The yellow solution was concentrated under vacuum at −60 °C, transferred in a Schlenk tube, concentrated again (>5 mL) and crystallized at −77 °C.

Raman (−198 °C, 1064 scans): $\tilde{\nu}$ = 3049 (w), 3028 (w), 2989 (w), 2982 (w), 2959 (w), 2941 (w), 2918 (w), 1645 (w), 1618 (w), 1564 (w), 1476 (w), 1460 (w), 1449 (w), 1420 (w), 1373 (w), 1163 (w), 1005 (s), 966 (w), 930 (w), 797 (w), 720 (s), 617 (s), 301 (w), 266 (m), 164 (s), 93 (s), 70 (s).

IR (ATR, −70 °C, 32 scans): $\tilde{\nu}$ = 3075 (w), 3028 (w), 2957 (w), 1530 (w), 1484 (w), 1366 (m), 1274 (s), 1201 (m), 1177 (w), 1132 (s), 1114 (m), 1053 (m), 1040 (m), 962 (w), 950 (w), 917 (w), 891 (m), 847 (w), 791 (m), 767 (w), 718 (w), 701 (m), 681 (m), 651 (w), 620 (w), 535 (w), 521 (w), 451 (w).

$[NMe_3(C_6H_4(CF_3))]O_3$

The ion exchange resin Amberlyst® 15 (Merk) (3.4 g) was charged with 3-(Trifluoromethyl)phenyltrimethylammonium (>98%, TCI) and was placed inside a H-shaped glass apparatus (as mentioned above) and cooled with a dry ice ethanol bath to −70 °C and the potassium ozonide (ca. 120 mg, 1,38 mmol) was added. Afterwards, ammonia (ca. 15 mL) was condensed onto the solids at −196 °C and the mixture was allowed to warm to −60 °C to fully dissolve the ozonide. The solution was stored at −76 °C for 3 days and extracted 3 times as described before.[4] The red solution was concentrated under vacuum at −60 °C, transferred in a Schlenk tube, concentrated again (>8 mL) and crystallized at −77 °C.

$[NMe_3(C_6H_3(CH_3)_2)]O_3$

The ion exchange resin Amberlyst® 15 (Merk) (2.7 g) was charged with (3,5-dimethylphenyl)trimethylammonium and was placed inside a H-shaped glass apparatus (as mentioned above) and cooled with a dry ice ethanol bath to −70 °C and the potassium ozonide (ca. 100 mg, 1,15 mmol) was added. Afterwards, ammonia (ca. 15 mL) was condensed onto the solids at −196 °C and the mixture was allowed to warm to −60 °C to fully dissolve the ozonide. The solution was stored at −76 °C for 3 days and extracted 3 times as described before.[4] The red solution was concentrated under vacuum at −60 °C, transferred in a Schlenk tube, concentrated again (>6 mL) and crystallized at −77 °C.

Deposition Numbers CCDC: 2281403 for $[NMe_3(C_8F_6H_3)][ONOO]\cdot 1/3\ NH_3$, 2281402 for $[NMe_3(C_8F_3H_4)]O_3$, 2324928 for $[NMe_3(C_6H_3(CH_3)_2)]O_3$ and 2324374 for $[NMe_3(C_6H_3(CF_3)_2))][SO_3CF_3]\cdot 1/2\ NH_3$.

Supporting Information

The authors have cited additional references within the Supporting Information.[48]

Acknowledgements

We gratefully acknowledge the ERC Project HighPotOx (Grant agreement ID: 818862) and the Core Facility BioSupraMol supported by the DFG. We gratefully acknowledge the Zentraleinrichtung für Datenverarbeitung (ZEDAT) of the Freie Universität Berlin for the allocation of computing resources. The project was also supported by the Deutsche Forschungsgemeinschaft (DFG, German Research Foundation) – Project-ID 387284271 – SFB 1349. The authors like to thank Dr. Patrick Voßnacker for low temperature single crystal Raman measurements, Niklas Limberg for an XRD measurement, Dr. Julia Bader for low temperature NMR measurements, Dr. Günther Thiele for his valuable assistance in evaluating crystallographic data, Dr. Dirk Andrae and Dr. Carsten Müller for helpful discussions and

Gesa Dreyhsig for the TOC design. Open Access funding enabled and organized by Projekt DEAL.

Conflict of Interests

The authors declare no conflict of interest.

Data Availability Statement

The data that support the findings of this study are available in the supplementary material of this article.

Keywords: Ozonide · Peroxynitrite · Fluorine specific interactions · X-ray diffraction · Radicals

[1] M. Jansen, H. Nuss, *Z. Anorg. Allg. Chem.* **2007**, *633*, 1307.
[2] a) W. Schnick, M. Jansen, *Angew. Chem.* **1985**, *97*, 48; *Angew. Chem. Int. Ed.* **1985**, *24*, 54; b) W. Schnick, M. Jansen, *Z. Anorg. Allg. Chem.* **1986**, *532*, 37; c) W. Schnick, M. Jansen, *Rev. Chim. Miner.* **1987**, 446.
[3] a) W. Hesse, M. Jansen, *Angew. Chem.* **1988**, *100*, 1388; *Angew. Chem. Int. Ed.* **1988**, *27*, 1341; b) M. Jansen, W. Hesse, *Z. Anorg. Allg. Chem.* **1988**, *560*, 47.
[4] N. Korber, M. Jansen, *Chem. Ber.* **1992**, *125*, 1383.
[5] A. Sans, H. Nuss, S. Mohitkar, M. Jansen, *Z. Anorg. Allg. Chem.* **2017**, *643*, 357.
[6] J. R. Schmid, P. Voßnacker, M. Jansen, S. Riedel, *Z. Anorg. Allg. Chem.* **2022**, *648*, e202200225.
[7] K. Reichenbächer, H. I. Süss, J. Hulliger, *Chem. Soc. Rev.* **2005**, *34*, 22–30.
[8] a) D. S. Bohle, B. Hansert, S. C. Paulson, B. D. Smith, *J. Am. Chem. Soc.* **1994**, *116*, 7423; b) C. Szabó, H. Ischiropoulos, R. Radi, *Nat. Rev. Drug Discovery* **2007**, *6*, 662.
[9] B. Biswas, P. C. Singh, *J. Fluorine Chem.* **2020**, *235*, 109414.
[10] a) X. Auvray, C. Petipas, R. Anthore, I. Rico, A. Lattes, *J. Phys. Chem.* **1989**, *93*, 7458; b) D. Myers, Surfactant Science and Technology, John Wiley & Sons, Hoboken, New Jersey, **2006**.
[11] S. Bzik, M. Jansen, *Chem. Eur. J.* **2003**, *9*, 613.
[12] M. Wörle, P. Latal, R. Kissner, R. Nesper, W. H. Koppenol, *Chem. Res. Toxicol.* **1999**, *12*, 305.
[13] D. S. Bohle, P. A. Glassbrenner, B. Hansert, *Methods Enzymol.* **1996**, *269*, 302.
[14] W. Schnick, Ph. D. Thesis, Univ. Hannover **1986**.
[15] a) R. N. Dixon, *J. Chem. Phys.* **1996**, *104*, 6905; b) J. R. B. Gomes, M. D. M. C. Ribeiro da Silva, M. A. V. Ribeiro da Silva, *J. Phys. Chem. A* **2004**, *108*, 2119.
[16] W. Klein, K. Armbruster, M. Jansen, *Chem. Commun.* **1998**, *6*, 707.
[17] N. Sieffert, A. Thakkar, M. Bühl, *Chem. Commun.* **2018**, *54*, 10431.
[18] a) W. Manchot, W. Kampschulte, *Ber. Dtsch. Chem. Ges.* **1907**, *40*, 4984; b) W. Manchot, *Ber. Dtsch. Chem. Ges. A* **1930**, *63*, 1225.
[19] H.-H. Tsai, T. P. Hamilton, J.-H. M. Tsai, M. van der Woerd, J. G. Harrison, M. J. Jablonsky, J. S. Beckman, W. H. Koppenol, *J. Phys. Chem.* **1996**, *100*, 15087.
[20] J.-H. M. Tsai, J. G. Harrison, J. C. Martin, T. P. Hamilton, M. van der Woerd, M. J. Jablonsky, J. S. Beckman, *J. Am. Chem. Soc.* **1994**, *116*, 4115.
[21] B. Liang, L. Andrews, *J. Am. Chem. Soc.* **2001**, *123*, 9848.
[22] K. F. Hoffmann, A. Wiesner, N. Subat, S. Steinhauer, S. Riedel, *Z. Anorg. Allg. Chem.* **2018**, *644*, 1344.
[23] M. C. González Lebrero, L. L. Perissinotti, D. A. Estrin, *J. Phys. Chem. A* **2005**, *109*, 9598.
[24] a) L. Krause, R. Herbst-Irmer, G. M. Sheldrick, D. Stalke, *J. Appl. Crystallogr.* **2015**, *48*, 3; b) APEX-IV (version 4.0), Data Reduction and Frame Integration Programfor the CCD Area-Detector System, Bruker AXS Inc.: Madison, Wisconsin (USA), **2021**.
[25] G. M. Sheldrick, *Acta Crystallogr.* **2015**, *A71*, 3.
[26] G. M. Sheldrick, *Acta Crystallogr.* **2015**, *C71*, 3.
[27] O. V. Dolomanov, L. J. Bourhis, R. J. Gildea, J. A. K. Howard, H. Puschmann, *J. Appl. Crystallogr.* **2009**, *42*, 339.
[28] DIAMOND (version 4.65), Crystal and Molecular Structure Visualization; Crystal Impact – Dr. H. Putz & Dr. K. Brandenburg GbR: Bonn (Germany), **2023**.
[29] OPUS (version 7.5); Bruker Optik GmbH: Ettlingen (Germany), **2014**.
[30] ORIGINPRO (version 9.9.0.220), Data Analysis and Graphing Software; OriginLab Corp.: Northampton, Massachusetts (USA), **2022**.
[31] R. K. Harris, E. D. Becker, S. M. Cabral de Menezes, P. Granger, R. E. Hoffman, K. W. Zilm, *Pure Appl. Chem.* **2008**, *80*, 59.
[32] MNOVA (version 14.3); Mestrelab Research, S. L.: Santiago de Compostela (Spain), **2022**.
[33] L. Bennett, B. Melchers, B. Proppe, *Freie Universität Berlin*, **2020**, published online, https://doi.org/10.17169/refubium-26754.
[34] a) F. Neese, *WIREs Comput. Mol. Sci.* **2011**, *2*, 73–78; b) F. Neese, *WIREs Comput. Mol. Sci.* **2022**, *12*, e1606.
[35] Gaussian (Gaussian 16), M. J. Frisch, G. W. Trucks, H. B. Schlegel, G. E. Scuseria, M. A. Robb, J. R. Cheeseman, G. Scalmani, V. Barone, G. A. Petersson, H. Nakatsuji, X. Li, M. Caricato, A. V. Marenich, J. Bloino, B. G. Janesko, R. Gomperts, B. Mennucci, H. P. Hratchian, J. V. Ortiz, A. F. Izmaylov, J. L. Sonnenberg, Williams, F. Ding, F. Lipparini, F. Egidi, J. Goings, B. Peng, A. Petrone, T. Henderson, D. Ranasinghe, V. G. Zakrzewski, J. Gao, N. Rega, G. Zheng, W. Liang, M. Hada, M. Ehara, K. Toyota, R. Fukuda, J. Hasegawa, M. Ishida, T. Nakajima, Y. Honda, O. Kitao, H. Nakai, T. Vreven, K. Throssell, J. A. Montgomery Jr., J. E. Peralta, F. Ogliaro, M. J. Bearpark, J. J. Heyd, E. N. Brothers, K. N. Kudin, V. N. Staroverov, T. A. Keith, R. Kobayashi, J. Normand, K. Raghavachari, A. P. Rendell, J. C. Burant, S. S. Iyengar, J. Tomasi, M. Cossi, J. M. Millam, M. Klene, C. Adamo, R. Cammi, J. W. Ochterski, R. L. Martin, K. Morokuma, O. Farkas, J. B. Foresman, D. J. Fox, Wallingford, CT, **2016**.
[36] a) A. D. Becke, *Phys. Rev. A.* **1988**, *38*, 3098; b) C. Lee, W. Yang, R. G. Parr, *Phys. Rev. B* **1988**, *37*, 785; c) S. Grimme, J. Antony, S. Ehrlich, H. Krieg, *J. Chem. Phys.* **2010**, *132*, 154104; d) S. Grimme, S. Ehrlich, L. Goerigk, *J. Comput. Chem.* **2011**, *32*, 1456.
[37] E. Caldeweyher, S. Ehlert, A. Hansen, H. Neugebauer, S. Spicher, C. Bannwarth, S. Grimme, *J. Chem. Phys.* **2019**, *150*, 154122.
[38] S. Grimme, *J. Chem. Phys.* **2006**, *124*, 034108.
[39] C. Adamo, V. Barone, *J. Chem. Phys.* **1999**, *110*, 6158.
[40] a) G. D. Purvis, III, R. J. Bartlett, *J. Chem. Phys.* **1982**, *76*, 1910; b) K. Raghavachari, G. W. Trucks, J. A. Pople, M. Head-Gordon, *Chem. Phys. Lett.* **1989**, *157*, 479.
[41] R. A. Kendall, T. H. Dunning Jr., R. J. Harrison, *J. Chem. Phys.* **1992**, *96*, 6796.
[42] NBO (NBO 7.0), E. D. Glendening, J. K. Badenhoop, A. E. Reed, J. E. Carpenter, J. A. Bohmann, C. M. Morales, P. Karafiloglou, C. R. Landis, F. Weinhold, Theoretical Chemistry Institute, University of Wisconsin, Madison **2018**.
[43] V. Ásgeirsson, B. O. Birgisson, R. Bjornsson, U. Becker, F. Neese, C. Riplinger, H. Jónsson, *J. Chem. Theory Comput.* **2021**, *17*, 4929.
[44] P. R. Spackman, M. J. Turner, J. J. McKinnon, S. K. Wolff, D. J. Grimwood, D. Jayatilaka, M. A. Spackman, *J. Appl. Crystallogr.* **2021**, *54*, 1006.
[45] W. Humphrey, A. Dalke, K. Schulten, *J. Mol. Graphics* **1996**, *14*, 33.
[46] J. R. Schmid, A. Wiesner, P. Voßnacker, M. Jansen, S. Riedel, *Z. Naturforsch. B* **2024**, *79*, 57.
[47] A. Hogg, M. Wheatley, P. Domingo-Legarda, A. Carral-Menoyo, N. Cottam, I. Larrosa, *JACS Au* **2022**, *2*, 2529.
[48] T. Lu, F. Chen, *J. Comput. Chem.* **2012**, *33*, 580.
[49] J.-M. Mewes, P. Jerabek, D. S. Bohle, P. Schwerdtfeger, *ChemPhotoChem* **2018**, *2*, 725.

Manuscript received: February 13, 2024
Accepted manuscript online: March 28, 2024
Version of record online: May 2, 2024